Research Square

Preprints are preliminary reports that have not undergone peer review.
They should not be considered conclusive, used to inform clinical practice,
or referenced by the media as validated information.

Inducible T-Cell Co-Stimulator Emerges During Chronic Liver Disease Progression and Defines a T-Cell–Inflamed Immune State in Hepatocellular Carcinoma

Grifton Tafadzwa Muchovu
20063791@studenti.uniupo.it

Università del Piemonte Orientale
Jean Francois Regis Igiramaboko
Trenholm State Community College
Hilarie Uwamahoro
Tuskegee University
Concorde Niyigaba Isange
Università del Piemonte Orientale
Pouya Bozorgpouryazdi
Università del Piemonte Orientale

Research Article

Keywords: HCC, ICOS, immune remodeling, TCGA, transcriptomics

Posted Date: March 24th, 2026

DOI: https://doi.org/10.21203/rs.3.rs-9060848/v1

License: This work is licensed under a Creative Commons Attribution 4.0 International License.
Read Full License

Additional Declarations: No competing interests reported.

Abstract

Background

Hepatocellular carcinoma (HCC) arises within chronic liver disease and is molded by complex immune remodeling. Inducible T-cell costimulator (ICOS) is an immune checkpoint associated with T-cell activation, but its timing and role across disease progression remain unclear. This study aimed to clarify the stage-specific regulation of ICOS and determine its role in molding immune architecture during hepatocellular carcinoma development.

Methods

We conducted staged transcriptomic profiling integrating early metabolic liver dysfunction (GSE89632), advanced inflammatory remodeling and HCC (GSE164760), and external validation in The Cancer Genome Atlas Liver Hepatocellular Carcinoma cohort (TCGA-LIHC). ICOS dynamics were evaluated across disease stages, followed by pathway enrichment, immune signature profiling, multivariable modeling, and unsupervised immune ecosystem stratification.

Results

ICOS expression was stable in early disease but increased significantly during advanced inflammatory remodeling and malignant transformation. ICOS-high tumors exhibited coordinated enrichment of interferon, costimulatory, inhibitory, and effector T-cell programs, showing a stable T-cell–inflamed immune architecture. In TCGA-LIHC, ICOS expression was independent of viral etiology and tumor stage but remained tightly associated with immune exhaustion signatures after multivariable adjustment. Unsupervised clustering defined an ICOS-enriched immune subtype, distinct from tumor burden and not independently predictive of survival.

Conclusions

ICOS emerges during advanced liver disease and remains as a structural regulator of immune architecture in HCC. These outcomes position ICOS as a marker of immune ecosystem state rather than tumor progression per se. Looking ahead, ICOS-defined immune states could serve as a practical basis for stratifying patients in future interventional studies, enabling personalized selection for ICOS agonist or antagonist therapies.

Introduction

Hepatocellular carcinoma (HCC) is the sixth most diagnosed cancer and the third leading cause of cancer-related death worldwide [1]. It is driven by both viral hepatitis and the increasing prevalence of

metabolic dysfunction–associated steatotic liver disease (MASLD) [2, 3]. MASLD can progress to metabolic dysfunction–associated steatohepatitis (MASH), advanced fibrosis, cirrhosis, and ultimately HCC through a multifaceted interaction of metabolic injury, chronic inflammation, and immune dysregulation [4]. The growing prevalence of MASLD-associated HCC underscores the need to better understand immune regulatory mechanisms that function across disease stages [3, 4].

The liver is immunologically unique. It maintains tolerance and mounts adaptive immune responses [5]. Chronic liver inflammation disturbs this balance, resulting in sustained inflammation and remodeling of the immune microenvironment [5, 6]. Previous studies using single-cell transcriptomics have shown substantial heterogeneity among tumor-infiltrating immune cells [7, 8]. This includes the coexistence of T-cell activation, dysfunction, and exhaustion states [7, 9]. Chronic inflammation is defined by T-cell exhaustion, sustained expression of inhibitory receptors, and transcriptional reprogramming [9]. These immune adaptations are clinically relevant, as demonstrated by the survival benefit of immune checkpoint blockade in advanced HCC [10].

Among costimulatory receptors, inducible T-cell co-stimulator (ICOS) has attracted increasing attention [11]. ICOS belongs to the CD28 family and plays a role in T-cell activation, maintenance, and differentiation [11, 12]. Its signalling contributes to follicular helper T-cell development, cytokine production, and immune regulation [12]. In cancer, ICOS is recognized for its double-edged role [13]. On one side, ICOS supports classical effector functions, including activation and persistence of T cells within the tumour microenvironment [13]. On the other hand, ICOS signalling also promotes regulatory T-cell expansion, which can dampen anti-tumour immunity [13, 16]. The most decisive findings from recent studies emphasize that ICOS expression marks distinct T-cell states within inflamed tumours, bridging effector activity with regulatory and exhaustion programs [15]. In HCC, where chronic antigen exposure and inflammatory remodelling are pervasive, ICOS may operate as part of coordinated immune architectures, rather than as an isolated checkpoint molecule [16].

Despite growing interest in ICOS for use in immunotherapy, its regulation in a spectrum of metabolic liver diseases remains unclear [16, 17]. Most investigations evaluate ICOS within established malignancy or experimental models, without resolving whether dysregulation begins during early metabolic dysfunction, arises during fibrotic remodeling, or primarily accompanies malignant transformation [16, 18]. A key unanswered question is: at what point during disease progression does ICOS expression diverge from that of its ligand, ICOSLG? Does this dissociation mark a pivotal event in immune microenvironment remodeling, or do ICOS and ICOSLG maintain synchronous transcriptional dynamics across the chronic liver disease spectrum? It is also still unclear whether ICOS reflects tumor burden and anatomical stage, or whether it instead defines a conserved immune microenvironment state independent of tumor progression [5]. The transcriptional behavior of its ligand, ICOSLG, across progressive liver disease is even less characterized, despite frequent assumptions of coordinated receptor–ligand regulation [17]. By framing these gaps as concrete, testable questions, this study aims to invite the reader directly into the scientific inquiry underlying our experimental approach.

Clarifying the stage-specific emergence of ICOS is necessary for interpreting its biological and translational significance [19]. Misattributing late-stage immune remodeling features to early pathogenic mechanisms may conceal the true sequence of immune adaptation during hepatocarcinogenesis [7]. A stage-resolved analysis is therefore necessary to define when ICOS dysregulation arises and whether it reflects structural immune remodeling rather than tumor expansion alone [19, 7].

We hypothesized that ICOS dysregulation does not occur during early metabolic dysfunction but instead emerges during advanced inflammatory remodeling and malignant transformation. We further hypothesized that once induced, ICOS becomes embedded within a coordinated T-cell–inflamed immune architecture independent of tumor stage and etiology.

To test these hypotheses, we performed, to our knowledge, the first multi-cohort study mapping ICOS emergence across the entire liver disease continuum. This staged multi-cohort transcriptomic investigation integrates early metabolic liver disease datasets, advanced inflammatory and HCC cohorts, and independent validation in the TCGA-LIHC dataset. Through pathway enrichment, immune signature profiling, multivariable modeling, and unsupervised immune ecosystem stratification, we sought to define the temporal emergence and biological positioning of ICOS across chronic liver disease progression and hepatocellular carcinoma. The conceptual framework guiding this study is illustrated in Fig. 1A.

Methodology

Study Design and Analytical Scheme

This study was conducted as a staged, multi-cohort transcriptomic investigation. The main objective was to define the temporal and stage-dependent regulation of ICOS across metabolic liver disease progression and hepatocellular carcinoma (HCC). It was hypothesized that ICOS dysregulation arises during advanced inflammatory remodeling and malignant transformation, rather than during early metabolic dysfunction. Furthermore, it was posited that, in these later stages, ICOS dysregulation appears associated with coordinated reprogramming of the immune microenvironment.

To test these hypotheses, a two-phase analytical scheme was implemented. In the first phase, transcriptomic profiling was performed across early and advanced metabolic liver disease using independent human liver microarray datasets. ICOS and ICOSLG expression dynamics, immune pathway enrichment, and immune gene signature remodeling in hepatocellular carcinoma were evaluated. The second phase validated these outcomes using an independent TCGA-LIHC cohort to assess tumor-stage independence, immune exhaustion coupling, multivariable modeling, interaction testing, survival analysis, and immune ecosystem stratification.

Statistical Model

All analyses were conducted in Python using pandas, NumPy, SciPy, statsmodels, lifelines, scikit-learn, seaborn, matplotlib, and gseapy. All tests were two-sided, with nominal significance defined as $p < 0.05$. Where applicable, Benjamini–Hochberg correction was applied.

Phase 1: Transcriptomic Analysis of ICOS Regulation in Metabolic Liver Disease

Dataset Selection

Human liver transcriptomic datasets were retrieved from the Gene Expression Omnibus (GEO). Inclusion criteria were: (i) human liver tissue, (ii) representation of both non-malignant and malignant disease states, (iii) available stage annotation, and (iv) platform-specific probe annotation files.

Two datasets met the criteria. GSE89632 (GPL14951; Illumina HumanHT-12) served as the early disease validation cohort. It included Healthy (n = 24), MASLD (n = 20), and MASH (n = 19) samples (n = 63 total). GSE164760 (GPL13667; Affymetrix Human Genome U219) served as the advanced disease discovery cohort and included Healthy (n = 6), NASH (n = 74), Cirrhosis (n = 8), Adjacent tissue (n = 29), and HCC tumors (n = 53) (n = 170 total).

Probe Processing and Gene-Level Collapsing

Series matrix files were downloaded from GEO, and platform-specific annotation files (GPL14951 and GPL13667) were used for probe-to-gene mapping. Probes without valid gene symbols were excluded. When multiple probes mapped to a single gene, expression values were collapsed using the median probe values. Expression values were retained on the log2-normalized scale. No cross-dataset normalization or batch correction was performed, as each dataset was analyzed independently.

Disease Stage Classification

Stage groups were derived from curated GEO annotations. For the GSE89632 cohort, samples were grouped as Healthy, MASLD, or MASH. In GSE164760, samples were categorized as Healthy, NASH, Cirrhosis, Adjacent non-tumoral tissue, or HCC tumor. GSM accession identifiers were used as unique keys for merging metadata with gene expression matrices.

ICOS and ICOSLG Expression Analysis

ICOS and ICOSLG expression values were extracted from gene-level matrices. Distributional assessment confirmed non-normal expression. For this reason, Kruskal–Wallis testing was used for multi-group comparisons. In GSE89632, expressions were compared across Healthy, MASLD, and MASH. As for the

GSE164760, cohort comparisons were done across Healthy, NASH, Cirrhosis, Adjacent, and Tumor groups. Pairwise median differences were calculated to quantify directional shifts across stages.

ICOS Stratification in HCC

HCC tumors (n = 53) in GSE164760 were dichotomized into ICOS-High and ICOS-Low groups using the median ICOS expression cutoff to preserve balanced group sizes and maximize statistical power for downstream analyses. The decision to use the median rather than a fixed percentile or quartile cutoff was based on the relatively small cohort size, which enabled reliable comparisons between groups of equal size while minimizing potential bias from arbitrary thresholds. Importantly, the median split approach has been commonly employed in transcriptomic analysis to facilitate reproducibility and clear reporting. Group separation was confirmed using the Mann–Whitney U test.

Pathway Enrichment Analysis

Pre-ranked Gene Set Enrichment Analysis (GSEA) was performed using the MSigDB Hallmark 2020 collection. Genes were ranked by the delta-median expression difference between ICOS-High and ICOS-Low tumors. Enrichment was performed using 1,000 permutations, with gene set size thresholds of 15–500 genes. False discovery rate (FDR) $q < 0.25$ was considered significant.

Immune Signature Profiling

Curated immune gene panels representing T-cell activation, exhaustion, costimulatory checkpoints, inhibitory checkpoints, and cytokine–chemokine signaling were assembled from immuno-oncology literature. For each tumor sample, signature scores were calculated as the mean log2 expression of genes within each panel. Group comparisons were performed using Mann–Whitney U testing with Benjamini–Hochberg correction.

In addition to group-level comparisons, tumor-level visualization of immune architecture was performed using the full gene expression matrix. Selected immune regulatory genes were extracted, standardized using z-score normalization, and hierarchically clustered to evaluate coordinated immune remodeling across ICOS-defined tumor subsets.

Phase 2: Validation, Multivariable Modeling, and Immune Ecosystem Stratification in TCGA-LIHC

TCGA Data Acquisition and Harmonization

RNA sequencing data (RNASeqV2, log2-normalized) and clinical annotations were obtained from the UCSC Xena portal for the TCGA-LIHC dataset. Clinical variables included overall survival and pathological tumor stage. Molecular and clinical data were merged using the first twelve characters of

TCGA barcodes. Samples lacking stage or survival data were excluded from stage-adjusted and survival analyses. All analyses used provided log2-normalized expression values without further transformation.

Tumor stage was extracted from and harmonized into an ordinal numeric variable (Stage I–IV). Substages were collapsed into primary-stage categories to preserve ordering and ensure adequate sample sizes per group.

Etiology and Stage Association

Tumors were stratified into viral and non-viral groups using viral hepatitis serology annotations. Differences in ICOS expression between etiologic groups were assessed using the Mann–Whitney U test. Associations between ICOS expression and tumor stage were evaluated using Spearman's rank correlation and Kruskal–Wallis testing. Differences in correlation strength were evaluated using Fisher's r-to-z transformation.

Immune Functional Score Construction

Composite transcriptional scores were constructed to quantify immune architecture. The exhaustion score was defined as the mean log2 expression of PDCD1, CTLA4, LAG3, TIGIT, and HAVCR2. The Treg score was calculated as the mean expression of FOXP3, IL2RA, and CTLA4. The CD8 score was computed using the mean expression of CD8A and CD8B. A Treg/CD8 balance metric was calculated by subtracting the CD8 score from the Treg score. The calculations were computed using vectorized operations.

Multivariable Modeling of Exhaustion Architecture

Ordinary least squares (OLS) regression was used to evaluate whether ICOS independently predicts exhaustion architecture. The primary model specification was:

Exhaustion score ~ ICOS expression + Stage numeric

Regression coefficients (β), 95% confidence intervals, R^2, and F-statistics were calculated using statsmodels. To test stage-dependent modulation of immune coupling, an interaction term was introduced:

Exhaustion score ~ ICOS expression + Stage numeric + (ICOS expression × Stage numeric)

A non-significant interaction term was interpreted as evidence of stage-independent ICOS–exhaustion coupling.

Survival Modeling

Cox proportional hazards regression was performed using overall survival as the endpoint. Two prespecified models were fitted:

Model 1: OS ~ ICOS expression + Stage numeric

Model 2: OS ~ ICOS expression + Stage numeric + Exhaustion score

Hazard ratios (HR), 95% confidence intervals, Wald p-values, concordance index (C-index), and partial Akaike Information Criterion (AIC) were calculated using lifelines. Kaplan–Meier survival curves were generated using median ICOS dichotomization and compared using the log-rank test.

Immune Ecosystem Stratification

To identify immune architectural subtypes, unsupervised k-means clustering was performed using standardized ICOS expression, exhaustion score, Treg score, and CD8 score. Features were z-score normalized using StandardScaler prior to clustering. Cluster number (k = 2–5) was assessed using silhouette score analysis. The optimal solution was selected based on the maximal silhouette coefficient.

Cluster-level mean values of immune features were calculated to characterize biological subtypes. Principal component analysis (PCA) was applied to visualize cluster separation in reduced-dimensional space. Kaplan–Meier analysis was used to evaluate survival differences across immune clusters.

Results

Section 1: Stage-Dependent Transcriptional Remodeling of ICOS Across Metabolic Liver Disease and HCC

Results Overview

The temporal emergence of ICOS dysregulation during the progression of metabolic liver disease was delineated using a staged analytical approach that integrated early metabolic dysfunction (GSE89632) and advanced inflammatory remodeling in hepatocellular carcinoma (GSE164760). This section is organized into three components: (i) evaluation of ICOS and ICOSLG expression in early metabolic disease, (ii) stage-resolved transcriptional dynamics across advanced liver pathology and HCC, and (iii) immune pathway and gene-level remodeling in ICOS-stratified tumors. Collectively, these analyses establish the timing of ICOS dysregulation and clarify whether it represents isolated gene activation or coordinated immune reprogramming. All figures and Supplementary tables are summarized in Table S0.

ICOS and ICOSLG Remain Stable During Early Metabolic Dysfunction

ICOS and ICOSLG expression were evaluated across Healthy (n = 24), MASLD (n = 20), and MASH (n = 19) liver samples in GSE89632 to determine whether ICOS dysregulation initiates during early metabolic perturbation.

ICOS expression demonstrated no significant difference across early disease states (Kruskal–Wallis H = 0.842, p = 0.656). Median expression values were comparable across groups, with overlapping

interquartile ranges and no directional shift (Fig. 1B). Similarly, ICOSLG expression remained transcriptionally stable (H = 0.969, p = 0.615; Fig. 1C). Descriptive statistics are in Table S1. These findings demonstrate that neither ICOS nor its ligand, ICOSLG, undergoes transcriptional modulation during early metabolic liver disease, indicating that dysregulation is not initiated during the initial steatotic or inflammatory transitions.

ICOS Becomes Dysregulated During Advanced Inflammatory Remodeling and Malignant Transformation

In contrast to early disease stability, ICOS expression varied substantially across advanced pathological stages in GSE164760 (Healthy n = 6; NASH n = 74; Cirrhosis n = 8; Adjacent n = 29; Tumor n = 53).

The Kruskal–Wallis test showed significant stage-dependent variation (H = 12.617, p = 0.013; Table S1). Median ICOS expression progressively increased from non-malignant liver to cirrhosis and adjacent tissue, with sustained elevation in tumor samples (Fig. 2A). These results suggest a progressive immunological shift rather than a single event. Directional pairwise median comparisons (Fig. 2B) revealed upward shifts from NASH to cirrhosis and from cirrhosis to adjacent tissue. Tumor samples displayed heterogeneous but persistently elevated ICOS levels relative to early-stage metabolic disease. Full pairwise statistics are reported in Table S2.

Kernel density analysis also supported a rightward distributional shift in cirrhotic and tumor samples relative to healthy liver (Fig. 2C). Adjacent tissue exhibited intermediate expression patterns, consistent with progressive microenvironment remodeling during chronic inflammation.

Importantly, ICOSLG did not vary substantially across advanced stages (H = 3.443, p = 0.486; Table S1) indicating receptor–ligand divergence during disease progression.

Collectively, these findings show that ICOS dysregulation emerges during advanced inflammatory remodeling and persists into hepatocellular carcinoma, whereas ICOSLG remains transcriptionally stable. This divergence implies receptor-specific immune regulatory amplification rather than coordinated ligand upregulation.

ICOS-High Tumors showed Coordinated Immune Pathway and Gene-Level Remodeling.

HCC tumors were stratified into ICOS-High (n = 27) and ICOS-Low (n = 26) groups using a median cutoff to assess whether ICOS dysregulation remains associated with wider immune microenvironment remodeling. Pre-ranked GSEA showed significant enrichment of immune-related Hallmark pathways in ICOS-High tumors (normalized enrichment scores > 1.5; FDR q < 0.25), including interferon signaling, inflammatory response, and TNFα signaling via NF-κB (Fig. 3A). Complete enrichment statistics are provided in Table S3 and Table S4.

To quantify coordinated immune remodeling at the programmatic level, curated immune gene panels were used for evaluation. ICOS-High tumors demonstrated elevated signature scores across

costimulatory checkpoints, inhibitory checkpoints, T-cell activation, T-cell exhaustion, and cytokine–chemokine programs (Fig. 3B). The most pronounced difference was observed in costimulatory signaling (Δ median = 4.58; FDR = 0.0025), while inhibitory and activation programs showed concordant directional shifts (Table S5).

To evaluate immune architecture at the tumor level, a focused immune regulatory gene panel was extracted from the full expression matrix. After z-score normalization and hierarchical clustering, ICOS-High tumors exhibited coordinated upregulation of costimulatory receptors (ICOS, TNFRSF9, CD28), inhibitory checkpoints (PDCD1, CTLA4, LAG3, TIGIT, HAVCR2), effector activation genes (IFNG, GZMB, PRF1), and inflammatory chemokines (CXCL9, CXCL10, CCL5) (Fig. 3C).

Importantly, clustering demonstrated that these programs rise in concert rather than independently, indicating that ICOS dysregulation shows a coordinated immune regulatory state instead of isolated gene activation.

These data establish that ICOS enrichment in HCC is embedded within a wider T-cell–inflamed transcriptional architecture characterized by simultaneous activation and checkpoint engagement.

Section 2: External Validation, Architectural Stability, and Immune Ecosystem Stratification in TCGA-LIHC

Results Overview

Multi-layer validation in the TCGA-LIHC cohort was performed to determine whether ICOS-associated immune remodeling observed during metabolic liver disease progression persists within established malignancy and reflects conserved immune architecture rather than tumor burden. This validation framework interrogated (i) etiology and stage independence of ICOS expression, (ii) multivariable modeling of the ICOS–exhaustion axis and overall survival, and (iii) ecosystem-level immune stratification using unsupervised clustering. Collectively, these analyses establish whether ICOS functions as a tumor burden marker or as a structural determinant of immune architecture.

ICOS Is Independent of Etiology and Tumor Stage in TCGA HCC

We first examined whether ICOS expression differed between viral and non-viral hepatocellular carcinoma. ICOS expression distributions were comparable across etiologic groups (Mann–Whitney $p = 0.65$), with overlapping medians and interquartile ranges (Fig. 4A). The processed dataset supporting this analysis is provided in Table S6.

Despite the absence of etiologic differences in ICOS abundance, ICOS strongly correlated with immune exhaustion score in both viral ($\rho = 0.75$, $p < 0.001$) and non-viral tumors ($\rho = 0.72$, $p < 0.001$) (Fig. 4B–C). A direct statistical comparison using Fisher's r-to-z transformation showed no significant difference in

correlation strength ($z = 0.73$, $p = 0.47$), confirming the conservation of the ICOS–exhaustion axis across etiologies. The full comparative statistics are reported in Table S7.

We next evaluated whether ICOS expression escalates with tumor burden. Spearman correlation revealed no association between ICOS and pathologic stage ($\rho = 0.03$, $p = 0.37$). Stage-stratified scatter visualization (Fig. 4D) further demonstrated that ICOS–exhaustion coupling continues across stages without stage-dependent amplification. Stage-specific correlation coefficients are provided in Table S8.

In multivariable regression adjusting for tumor stage (Exhaustion score ~ ICOS expression + Stage numeric), ICOS remained a strong independent predictor of exhaustion architecture ($\beta = 0.555$, $p < 0.001$), whereas stage was not significant ($p = 0.89$). The model explained 49.8% of the variance in exhaustion ($R^2 = 0.498$). Detailed regression coefficients are provided in Table S10 and cross-validated in Table S9.

These data collectively show that ICOS structures immune exhaustion architecture independently of etiology and tumor stage, indicating architectural stability rather than tumor-burden dependence.

ICOS Does Not Independently Predict Overall Survival

Multivariable Cox proportional hazards models were constructed to determine whether ICOS-mediated immune remodeling is associated with clinical outcomes. In stage-adjusted survival analysis (OS ~ ICOS expression + Stage numeric), ICOS was not associated with overall survival (HR ≈ 1.00, $p = 0.87$), whereas tumor stage remained a significant predictor (HR ≈ 1.20 per stage increment, $p = 0.01$; concordance index = 0.55). Kaplan–Meier analysis confirmed no survival difference between ICOS-high and ICOS-low tumors (log-rank $p > 0.05$; Fig. 5A).

In the fully adjusted model containing exhaustion score (OS ~ ICOS expression + Stage numeric + Exhaustion score), neither ICOS ($p = 0.93$) nor exhaustion (HR ≈ 0.98, $p = 0.77$) independently predicted survival, whereas stage remained dominant ($p = 0.01$; concordance index = 0.52). Coefficients are provided in Table S10 and Table S11.

These relationships are summarized visually in Fig. 5B, which demonstrates that ICOS and exhaustion hazard ratios cross unity in both models. Together, these data indicate that ICOS-mediated immune polarization reflects tumor immune ecology instead of intrinsic tumor aggressiveness.

ICOS Marks T-Cell–Inflamed Tumors Without Preferential Regulatory Skewing

Transcriptional scores for regulatory T cells (Treg), CD8 cytotoxic T cells, and immune exhaustion were constructed to dissect immune composition.

ICOS expression correlated strongly with both Treg score ($\rho = 0.566$, $p \approx 1.2 \times 10^{-112}$) and CD8 score ($\rho = 0.503$, $p \approx 2.7 \times 10^{-111}$). Correlation statistics are provided in Table S12. Fisher's r-to-z comparison

demonstrated no significant difference between Treg and CD8 correlations ($z = 0.105$, $p = 0.917$), and ICOS did not correlate with the Treg/CD8 balance metric ($\rho = -0.023$, $p = 0.34$).

The immune architecture correlation matrix (Fig. 5C) illustrates coordinated upregulation of ICOS, exhaustion, Treg, and CD8 programs, with no preferential skewing toward suppressive dominance. These data demonstrate that ICOS marks globally T-cell–inflamed tumors rather than selectively regulatory-biased microenvironments.

Immune Ecosystem Stratification Identifies a T-Cell–Inflamed ICOS-High Subtype

Unsupervised k-means clustering was performed by standardized ICOS, exhaustion, Treg, and CD8 scores to evaluate whether ICOS defines higher-order immune states beyond linear associations. Silhouette analysis supported a two-cluster solution (silhouette score = 0.36). Cluster classifications are provided in Table S13.

Cluster 1 exhibited coordinated elevation of ICOS (mean 5.15), exhaustion (6.29), Treg (5.11), and CD8 (7.02), defining a T-cell–inflamed immune subtype. Cluster 0 demonstrated uniformly lower immune feature values (Fig. 6B). Principal component analysis confirmed partition along PC1 (Fig. 6A).

Despite a distinct immune profile, cluster membership did not independently forecast survival (log-rank $p = 0.26$; Fig. 6C). This data supports the notion that ICOS defines immunological framework states rather than prognostic tumor biology in untreated TCGA HCC.

Discussion

ICOS as a Stage-Emergent Architect of Immune Remodeling in HCC

This multi-cohort transcriptomic study shows that ICOS functions not solely as a marker of tumour burden or prognosis, but as a stage-emergent regulator of immune architecture in hepatocellular carcinoma (HCC). By combining early metabolic liver disease datasets, advanced inflammatory remodelling cohorts, and external validation in TCGA-LIHC, this study formulates a model in which ICOS dysregulation arises during advanced inflammatory transformation. Subsequently, ICOS stabilizes following malignancy and defines a conserved T-cell–inflamed immune ecosystem within established tumours. The results position ICOS as a structural determinant of the tumour microenvironment rather than a linear immune checkpoint molecule [11, 13].

ICOS Emerges Late in Disease Evolution

An important finding of this study is the temporal specificity of ICOS dysregulation. In early metabolic liver disease (MASLD and MASH), both ICOS and its ligand ICOSLG remained transcriptionally stable. Despite metabolic stress and inflammation, there was no evidence of progressive ICOS induction. These results suggest that ICOS is not involved in the initial immune perturbation associated with steatosis or early inflammatory activation, which are mainly driven by innate immune signaling and metabolic injury [3, 4].

In contrast, ICOS expression increased significantly during advanced pathological states, including cirrhosis, adjacent non-tumoral tissue, and HCC. The distributional shift across these stages was gradual rather than sudden. These observations support a model of progressive immune remodeling rather than oncogenic activation alone [19]. ICOSLG did not mirror this pattern, indicating receptor-specific amplification rather than coordinated ligand upregulation. These outcomes suggest that ICOS upregulation is linked to chronic inflammatory remodeling and the transition toward a tumor-permissive immune microenvironment [5, 6].

ICOS-High Tumors Exhibit Coordinated Immune Activation and Exhaustion

When HCC tumors were stratified by ICOS expression, ICOS-high tumors showed coordinated enrichment of interferon signaling, inflammatory response pathways, and TNFα–NFκB signaling. At the gene level, ICOS-high tumors showed simultaneous upregulation of costimulatory receptors, inhibitory checkpoints, cytotoxic effector genes, and inflammatory chemokines, with these programs rising together. This shows a synchronized T-cell–inflamed transcriptional state consistent with prior single-cell observations in HCC [7, 8]. Previous studies have characterized ICOS expression within established tumors or individual immune cell subsets, however our analysis demonstrates that ICOS-associated immune architecture emerges progressively during disease evolution and remains stable after malignant transformation.

Simultaneous elevations in activation and exhaustion signatures were observed, consistent with chronic antigen exposure and sustained immune engagement [9, 14]. The results support the interpretation that ICOS marks an immune microenvironment characterized by sustained T-cell activation alongside compensatory checkpoint regulation. Instead of representing immune suppression alone, ICOS appears to be embedded within a dynamic regulatory balance, a phenomenon well described in chronic inflammatory and cancer settings [9, 14].

Immune Architecture Is Independent of Etiology and Tumor Stage

Validation in TCGA-LIHC clarified that ICOS expression is independent of both viral etiology and pathological tumor stage. ICOS did not differ between viral and non-viral tumors and did not increase with anatomical stage progression. This dissociation is biologically meaningful. Tumor stage reflects macroscopic growth and invasion, whereas ICOS reflects the immune microenvironment state [6]. This

suggests that once established, ICOS-associated immune architecture remains stable throughout tumor evolution.

Despite this stage independence, ICOS consistently correlated with immune exhaustion across etiologies and stage strata. Multivariable modeling confirmed that ICOS independently predicts exhaustion architecture even after adjusting for tumor stage. Together, these data show that the ICOS–exhaustion axis is embedded within the tumor microenvironment and maintained irrespective of tumor burden, consistent with recognized models of exhaustion stability in chronic disease [14].

ICOS Shows a T-Cell–Inflamed State Without Preferential Regulatory Skewing

A key question is whether ICOS enrichment reflects preferential expansion of regulatory T cells. Prior studies have shown that ICOS can be expressed by both effector and regulatory T-cell subsets, depending on context [11, 13]. However, our data does not support selective regulatory dominance. ICOS correlated strongly with both Treg and CD8 cytotoxic signatures, and no association was observed with the Treg/CD8 balance metric.

Unsupervised clustering identified two immune ecosystems: an immune-low subtype and a T-cell–inflamed subtype characterized by coordinated elevation of ICOS, exhaustion, Treg, and CD8 programs. ICOS was enriched within the inflamed subtype but did not skew immune balance toward suppressive predominance. This is consistent with reports that ICOS functions as a context-dependent modulator of immune activation rather than an inherently suppressive signal [13, 16].

Thus, ICOS expression at the bulk tumor level likely reflects global T-cell engagement instead of selective regulatory expansion, consistent with tumor-infiltrating lymphocyte heterogeneity described in HCC [7]. These findings suggest that ICOS-defined immune states may represent biologically relevant contexts for future ICOS-targeted immunotherapies, where modulation of the ICOS pathway could potentially amplify pre-existing T-cell–inflamed tumor microenvironments.

Immune Remodeling Does Not Independently Predict Survival

Despite clear immune stratification, ICOS expression and immune cluster membership did not independently predict overall survival in TCGA. Tumor stage remained the major determinant of prognosis, consistent with established epidemiological and clinical observations in HCC [1, 2].

This highlights a biological separation between immune architecture and anatomical tumor progression. In largely untreated cohorts such as TCGA, tumor burden is expected to dominate survival outcomes [6]. Immune polarization may instead influence therapeutic responsiveness rather than baseline prognosis, notably in the context of immune checkpoint blockade [10, 17]. Therefore, ICOS-defined immune states

should be interpreted as markers of the immune context rather than as indicators of intrinsic tumor aggressiveness.

A Hierarchical Model of Immune Remodeling

The results support a hierarchical framework:

- ICOS is not induced during early metabolic dysfunction.
- It emerges during advanced inflammatory remodeling and malignant transformation.
- Within the established HCC, ICOS defines a stable T-cell–inflamed immune ecosystem.
- This immune architecture is independent of tumor stage and etiology.
- Immune ecosystem stratification does not independently determine survival in untreated cohorts.

This model clarifies the apparent paradox between disease-stage emergence and tumor-stage independence. ICOS is induced during inflammatory transformation instead of anatomical tumor expansion, consistent with progressive immune adaptation described in chronic liver disease and cancer immunology [5, 6, 14].

Limitations

This study is based on bulk transcriptomic data and therefore cannot resolve cell-type-specific ICOS expression or spatial immune organization. As a direct next step, single-cell and spatial profiling approaches—such as single-cell RNA sequencing and multiplex imaging—should be employed to dissect the cellular sources of ICOS and map its distribution within the liver tumor microenvironment [7, 8]. Additionally, trajectory inference methods could unravel the dynamics of immune cell state transitions during disease progression [7]. Another limitation is that the TCGA dataset predominantly reflects untreated tumors. Future studies should specifically examine immunotherapy-treated patient cohorts to determine whether ICOS-defined immune ecosystems can predict treatment responsiveness, especially in the context of immune checkpoint blockade, where T-cell inflamed states regularly forecast response [10, 17]. By prioritizing these directions, future research can address the current gaps and directly test the translational relevance of ICOS-associated immune states.

Conclusion

To sum up, ICOS functions as a stage-emergent architect of immune remodeling in hepatocellular carcinoma. It is induced during advanced inflammatory progression, persists following malignant transformation, and defines a conserved T-cell–inflamed tumor ecosystem independent of tumor stage and etiology. By reframing ICOS as a structural regulator of immune ecology rather than a simple checkpoint marker or prognostic factor, this study provides a mechanistic model linking chronic inflammatory liver disease to stable immune architecture in HCC.

Declarations

Conflict of Interest

The authors declare that they have no competing interests.

Clinical Trial Number

Clinical Trial Number not applicable

Funding Declaration

No funding was received for this project

Availability of Data and Materials

All data used in the project is publicly available on GEO repository. All supplementary data and figs that support this project are uploaded on Zenedo and can be accessed via the following link.
https://doi.org/10.5281/zenodo.18903688

Author Contributions

All authors contributed equally to the conception, design, and execution of the study. The overall manuscript was drafted and critically revised by all authors for important intellectual content. All authors read and approved the final manuscript.

Informed Consent

Informed consent was not required for this study, as it involved secondary analysis of publicly available, anonymised data.

References

1. Bray F, Laversanne M, Sung H, Ferlay J, Siegel RL, Soerjomataram I, Jemal A (2024) Global cancer statistics 2022: GLOBOCAN estimates of incidence and mortality worldwide for 36 cancers in 185 countries. Cancer J Clin 74(3):229–263. https://doi.org/10.3322/caac.21834
2. McGlynn KA, Petrick JL, El-Serag HB (2021) Epidemiology of hepatocellular carcinoma. Hepatology 73(S1):4–13. https://doi.org/10.1002/hep.31288
3. Younossi ZM, Kalligeros M, Henry L (2024) Epidemiology of metabolic dysfunction-associated steatotic liver disease. Clin Mol Hepatol 31(Suppl):S32. https://doi.org/10.3350/cmh.2024.0431
4. Estes C, Razavi H, Loomba R, Younossi Z, Sanyal AJ (2018) Modeling the epidemic of nonalcoholic fatty liver disease demonstrates an exponential increase in burden of disease. Hepatology 67(1):123–133. https://doi.org/10.1002/hep.29466
5. Pfister D, Núñez NG, Pinyol R, Govaere O, Pinter M, Szydlowska M, Gupta R, Qiu M, Deczkowska A, Weiner A et al (2021) NASH limits anti-tumour surveillance in immunotherapy-treated hepatocellular

carcinoma. Nature 592(7854):450–456. https://doi.org/10.1038/s41586-021-03362-0

6. Llovet JM, Kelley RK, Villanueva A, Singal AG, Pikarsky E, Roayaie S, Lencioni R, Koike K, Zucman-Rossi J, Finn RS (2021) Hepatocellular carcinoma. Nat Reviews Disease Primers 7:6. https://doi.org/10.1038/s41572-020-00240-3
7. Zhang Q, He Y, Luo N, Patel SJ, Gao R, Modak M, Carotta S, Haslinger C, Kind D, Van den Brink MRM et al (2019) Landscape and dynamics of single immune cells in hepatocellular carcinoma. Cell 179(4):829–845. https://doi.org/10.1016/j.cell.2019.10.003
8. Sun Y, Wu L, Zhong Y, Zhou K, Hou Y, Wang Z, Zhang Y, Wang Y, Zhang Y, Yuan J et al (2021) Single-cell landscape of the ecosystem in early-relapse hepatocellular carcinoma. Cell 184(2):404–421. https://doi.org/10.1016/j.cell.2020.11.041
9. Beltra JC, Manne S, Abdel-Hakeem MS, Kurachi M, Giles JR, Chen Z, Casella V, Ngiow SF, Khan O, Huang Y et al (2020) Developmental relationships of four exhausted CD8 T cell subsets reveal underlying transcriptional and epigenetic control mechanisms. Immunity 52(5):825–841. https://doi.org/10.1016/j.immuni.2020.04.014
10. Finn RS, Qin S, Ikeda M, Galle PR, Ducreux M, Kim TY, Kudo M, Breder V, Merle P, Kaseb AO et al (2020) Atezolizumab plus bevacizumab in unresectable hepatocellular carcinoma. N Engl J Med 382(20):1894–1905. https://doi.org/10.1056/NEJMoa1915745
11. Wikenheiser DJ, Stumhofer JS (2016) ICOS co-stimulation: Friend or foe? Front Immunol 7:304. https://doi.org/10.3389/fimmu.2016.00304
12. Crotty S (2019) T follicular helper cell biology: a decade of discovery and diseases. Immunity 50(5):1132–1148. https://doi.org/10.1016/j.immuni.2019.04.011
13. Amatore F, Gorvel L, Olive D (2020) Role of inducible co-stimulator (ICOS) in cancer immunotherapy. Expert Opin Biol Ther 20(2):141–150. https://doi.org/10.1080/14712598.2020.1693540
14. Blank CU, Haining WN, Held W, Hogan PG, Kallies A, Lugli E et al (2019) Defining 'T cell exhaustion'. Nat Rev Immunol 19(11):665–674. https://doi.org/10.1038/s41577-019-0221-9
15. Sade-Feldman M, Yizhak K, Bjorgaard SL, Ray JP, de Boer CG, Jenkins RW et al (2019) Defining T cell states associated with response to checkpoint immunotherapy in melanoma. Cell 176(1–2):404–419. https://doi.org/10.1016/j.cell.2018.12.034
16. Nikanjam M, Kato S, Nishizaki D et al (2026) Inducible T-cell co-stimulator (ICOS) and ICOS ligand: Dealing with a two-faced cancer immunoregulatory system. Cancer Med 15(1):e71467. https://doi.org/10.1002/cam4.71467
17. Shen KY, Zhu Y, Xie SZ et al (2024) Immunosuppressive tumor microenvironment and immunotherapy of hepatocellular carcinoma: Current status and perspectives. J Hematol Oncol 17:25. https://doi.org/10.1186/s13045-024-01549-2
18. Khan O, Giles JR, McDonald S et al (2019) TOX transcriptionally and epigenetically programs CD8 T cell exhaustion. Nature 571(7764):211–218. https://doi.org/10.1038/s41586-019-1325-x
19. Ma L, Hernandez MO, Zhao Y, Mehta M, Tran B, Kelly M et al (2019) Tumor cell biodiversity drives microenvironmental reprogramming in liver cancer. Cancer Cell 36(4):418–430.

https://doi.org/10.1016/j.ccell.2019.08.007

Figures

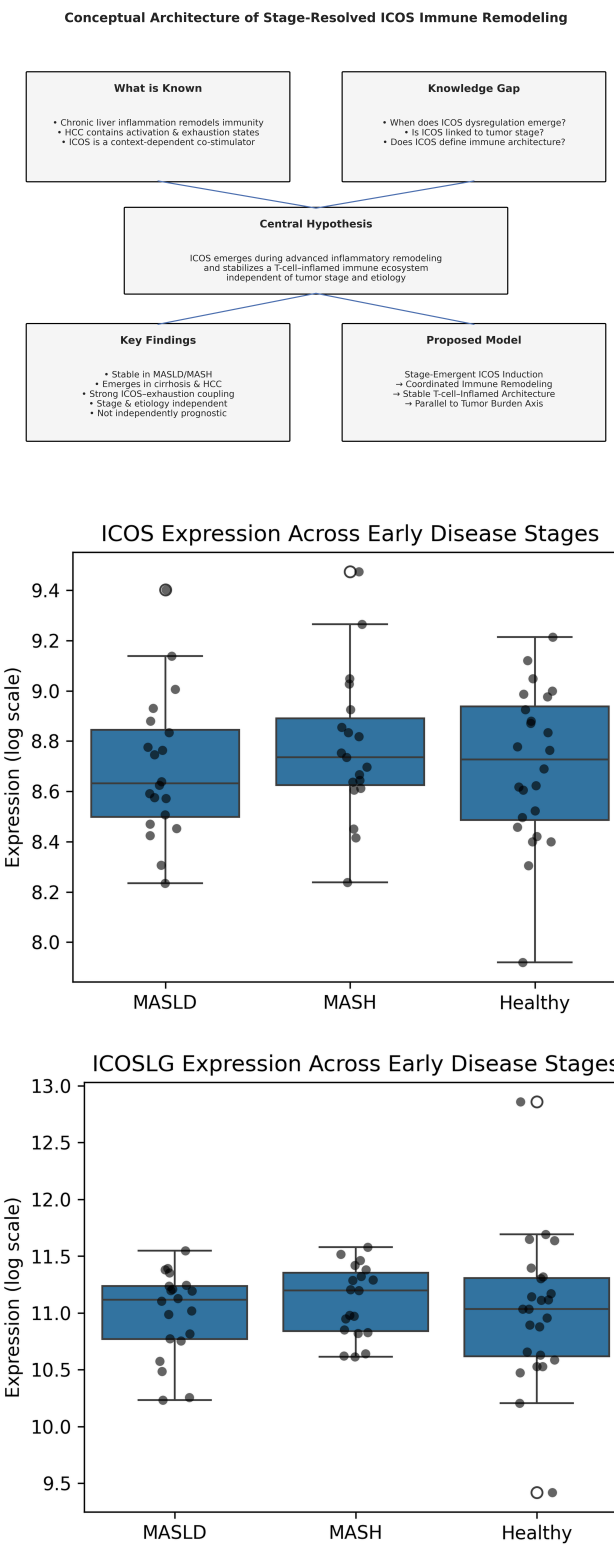


Figure 1

Conceptual framework and early-stage transcriptional stability of ICOS in metabolic liver disease (GSE89632). **(A)** Conceptual schematic summarizing the study rationale and central hypothesis that ICOS emerges during advanced inflammatory remodeling and stabilizes a T-cell–inflamed immune ecosystem independent of tumor stage and etiology. **(B)** ICOS expression across Healthy (n=24), MASLD (n=20), and MASH (n=19) liver samples. No significant differences were observed (Kruskal–Wallis H = 0.842, p = 0.656).**(C)** ICOSLG expression across the same early disease states. No significant differences were detected (Kruskal–Wallis H = 0.969, p = 0.615). Expression values represent log2-normalized microarray intensities. Boxes denote interquartile range (IQR), center lines indicate medians, and whiskers represent 1.5× IQR. Statistical testing was performed using Kruskal–Wallis analysis.

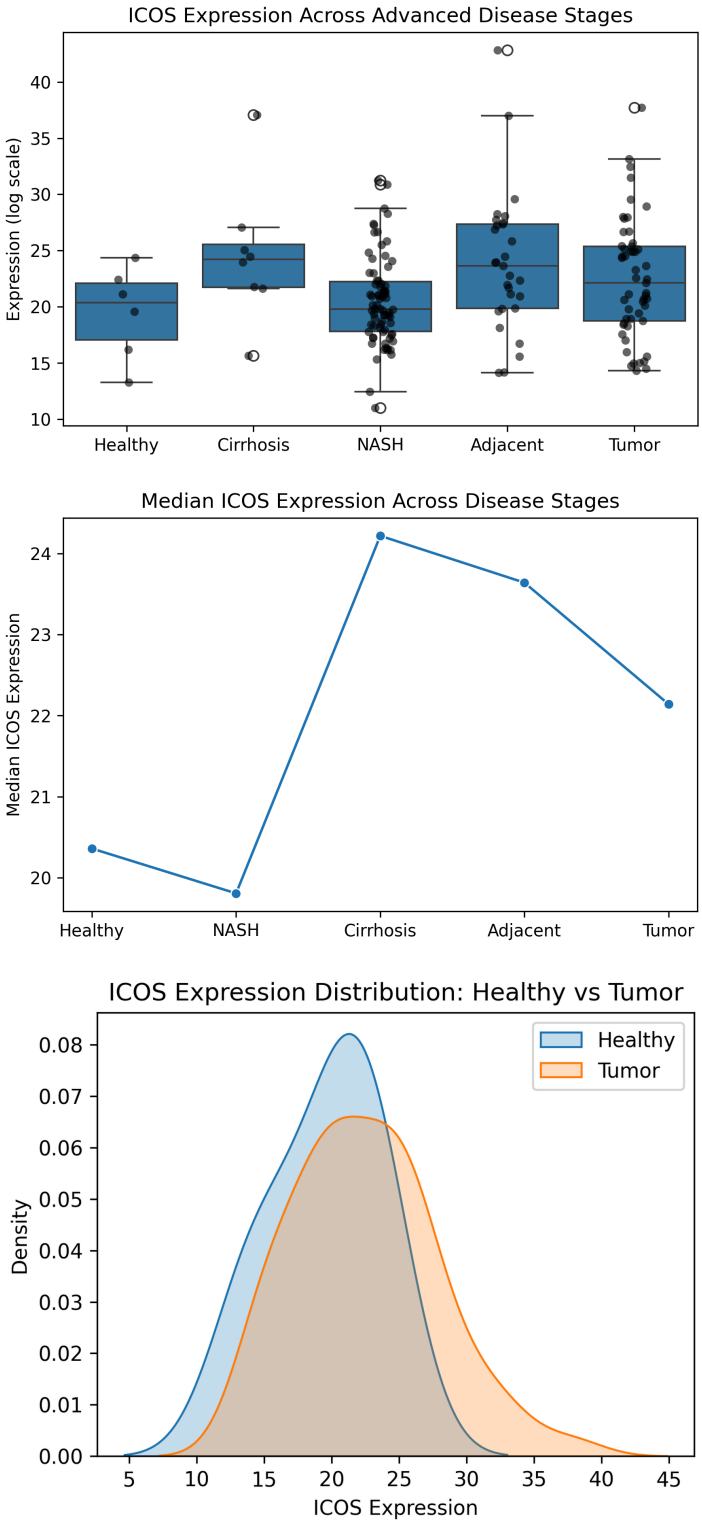
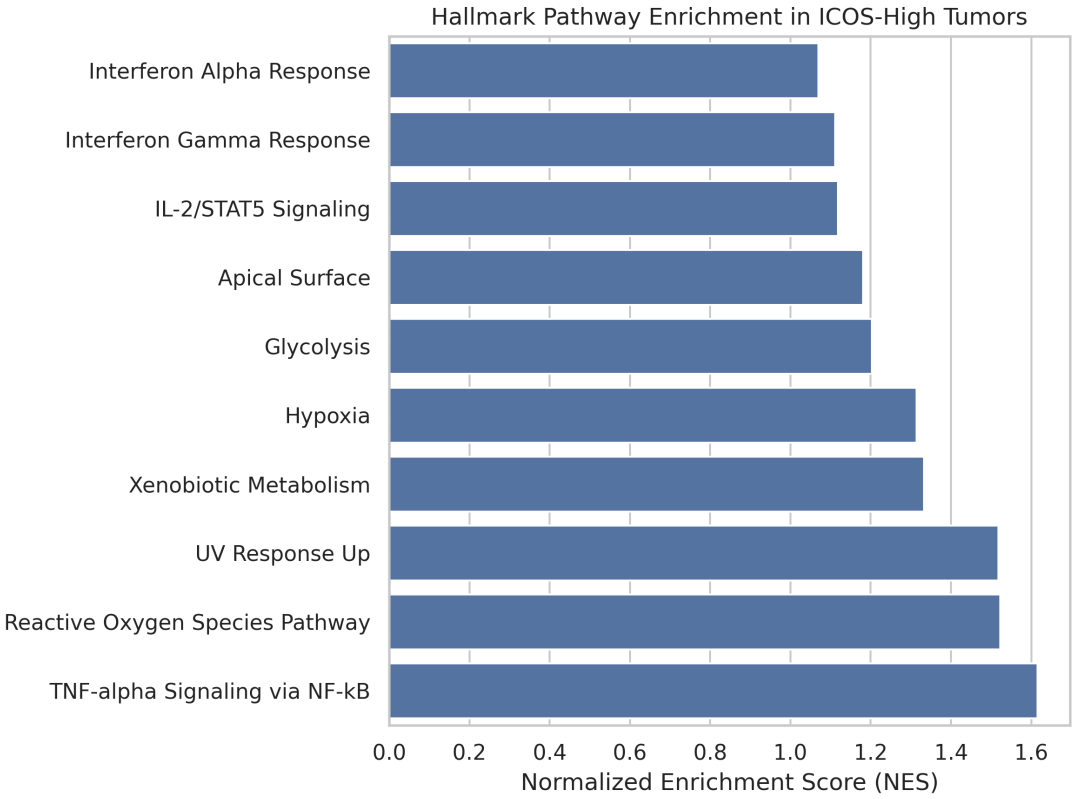


Figure 2

Stage-dependent emergence of ICOS dysregulation during advanced inflammatory remodeling and hepatocellular carcinoma (GSE164760). (A) Boxplot of ICOS expression across Healthy (n=6), NASH (n=74), Cirrhosis (n=8), Adjacent non-tumoral tissue (n=29), and HCC tumor samples (n=53). ICOS expression varied substantially across stages (Kruskal–Wallis H = 12.617, p = 0.013). (B) Pairwise median directional shifts illustrating progressive elevation of ICOS from NASH to cirrhosis and adjacent

tissue. Full pairwise statistics are provided in Supplementary Table S3. (C) Density distribution plot demonstrating rightward shift of ICOS expression in cirrhosis and tumor samples relative to healthy liver. Expression values are log2-normalized. These findings show that ICOS dysregulation emerges during advanced inflammatory remodeling and persists to malignancy.



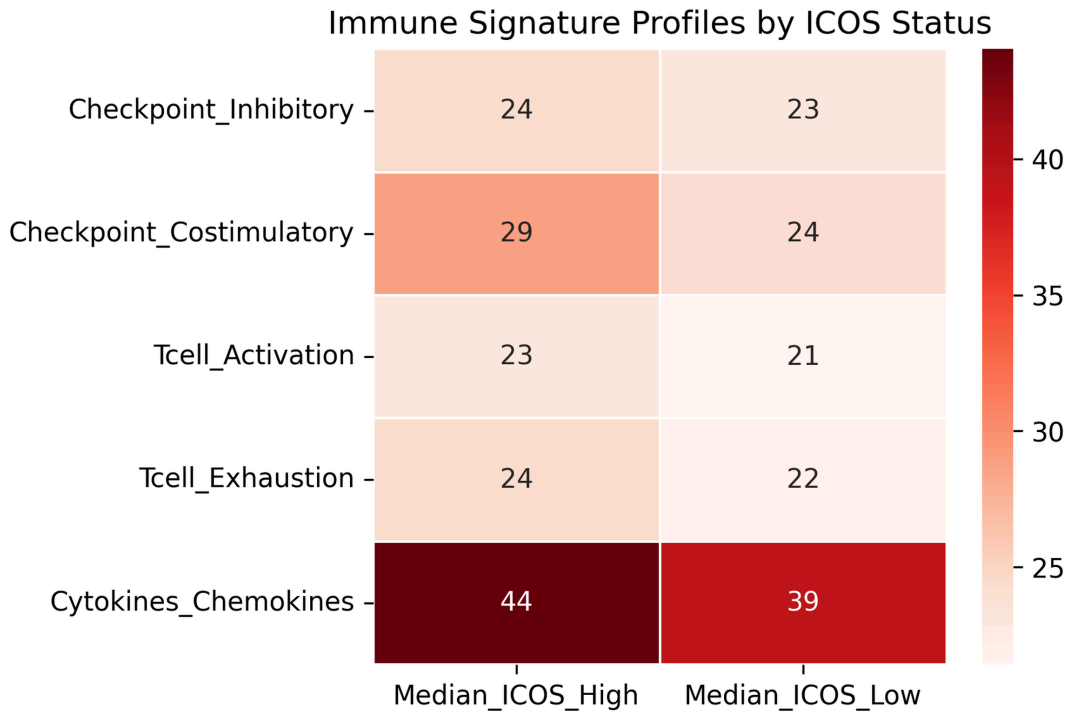


Figure 3

ICOS-high tumors exhibit coordinated immune pathways and gene-level remodeling. (A) Hallmark Gene Set Enrichment Analysis (GSEA) of ICOS-High versus ICOS-Low tumors. Immune-related pathways, including interferon signaling, inflammatory response, and TNFα signaling via NF-κB, were enriched in ICOS-High tumors (FDR $q < 0.25$). (B) Immune signature heatmap showing median program-level enrichment across costimulatory checkpoints, inhibitory checkpoints, T-cell activation, T-cell exhaustion, and cytokine–chemokine signaling. (C) Tumor-level immune gene heatmap (z-score normalized) demonstrating coordinated upregulation of costimulatory receptors (ICOS, TNFRSF9, CD28), inhibitory checkpoints (PDCD1, CTLA4, LAG3, TIGIT, HAVCR2), cytotoxic effectors (IFNG, GZMB, PRF1), and inflammatory chemokines (CXCL9, CXCL10, CCL5) in ICOS-High tumors. Together, these panels demonstrate that ICOS enrichment reflects coordinated immune remodeling instead of isolated gene activation.

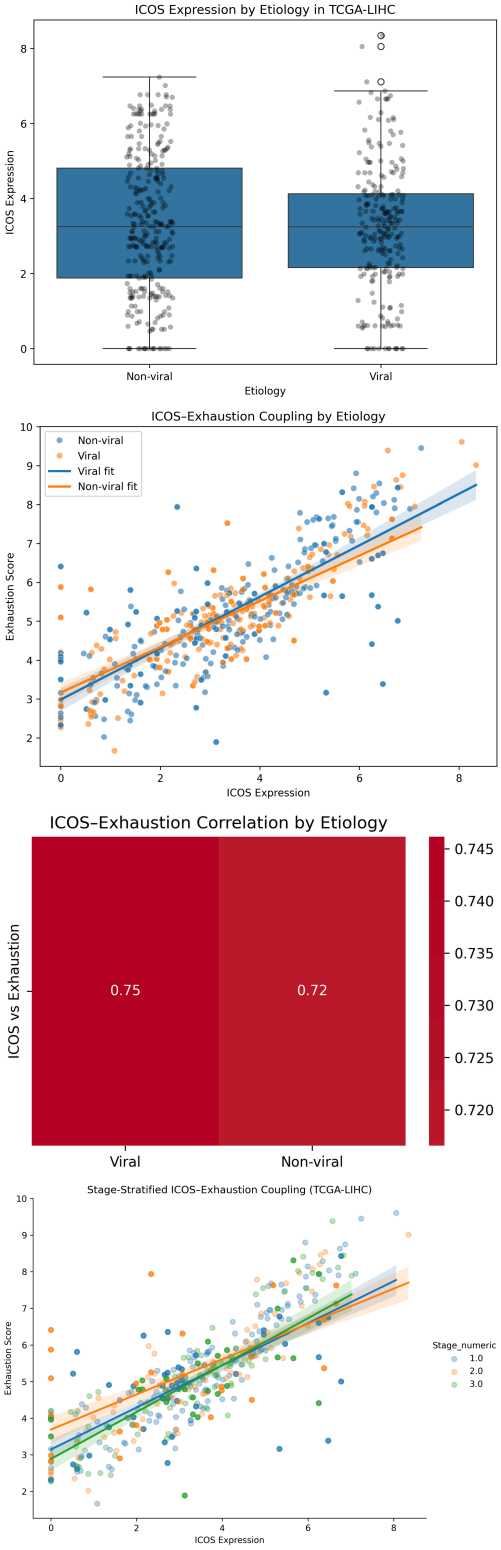


Figure 4

ICOS-associated immune architecture is independent of viral etiology and tumor stage in TCGA-LIHC. (A) ICOS expression by etiology (viral vs non-viral). No significant difference was observed (Mann–Whitney p = 0.65). (B) Correlation of ICOS with exhaustion score in viral tumors (ρ = 0.75, p < 0.001). (C) Correlation of ICOS with exhaustion score in non-viral tumors (ρ = 0.72, p < 0.001). No significant difference in

correlation strength (Fisher's z = 0.73, p = 0.47). These findings show that the ICOS–exhaustion axis is conserved across etiologies.

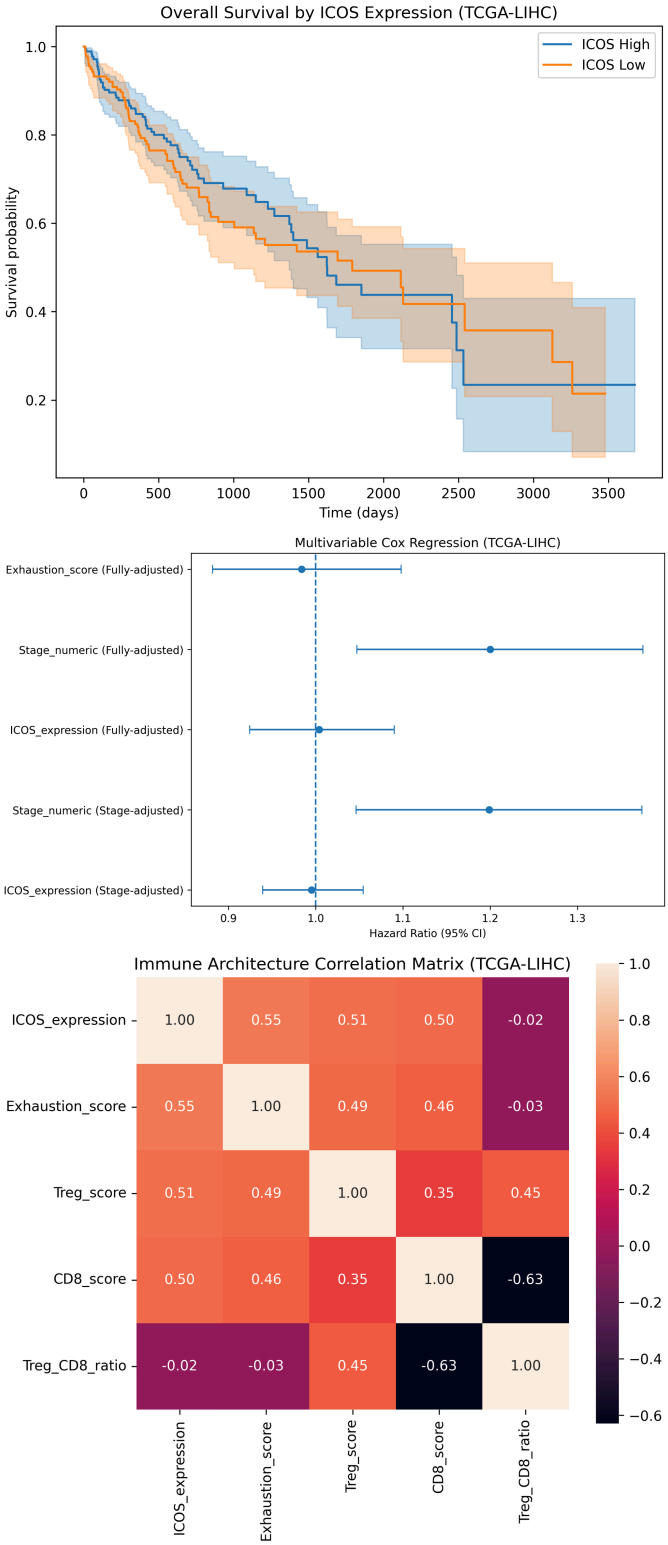


Figure 5

ICOS structures immune architecture but does not independently predict survival. (A) Kaplan–Meier survival curves comparing ICOS-High and ICOS-Low tumors (log-rank p > 0.05). (B) Multivariable Cox regression forest plot showing hazard ratios (HR) for ICOS expression and tumor stage. ICOS was not

independently associated with survival (HR ≈ 1.00, p > 0.05), whereas stage remained significant. (C) Immune architecture correlation matrix illustrating coordinated upregulation of ICOS, exhaustion, Treg, and CD8 programs. No preferential skewing toward Treg dominance was observed. These data indicate that ICOS reflects immune ecology instead of intrinsic tumor aggressiveness.

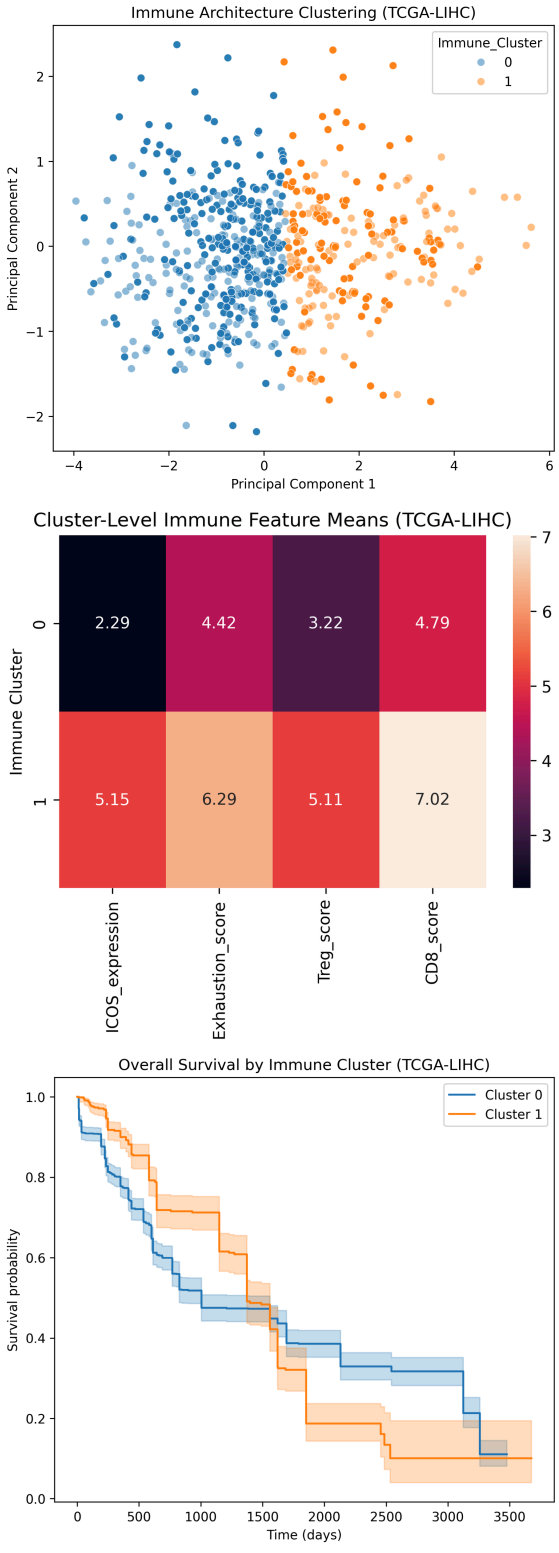


Figure 6

Unsupervised immune ecosystem stratification identifies an ICOS-enriched T-cell–inflamed subtype. (A) Principal component analysis (PCA) of standardized ICOS, exhaustion, Treg, and CD8 scores reveal two immune clusters. (B) Cluster-level immune feature heatmap demonstrating coordinated elevation of ICOS, exhaustion, Treg, and CD8 programs in Cluster 1 relative to Cluster 0. (C) Kaplan–Meier survival analysis by immune cluster showing no independent survival difference (log-rank p = 0.26). Silhouette analysis supported a two-cluster solution (silhouette score = 0.36). These data indicate that ICOS defines immune ecosystem states rather than prognostic tumor biology.

Supplementary Files

This is a list of supplementary files associated with this preprint. Click to download.

- TabelS1.xlsx
- TableS0.xlsx
- TableS3.xlsx
- TableS2.xlsx
- TableS4.xlsx
- TableS5.xlsx
- TableS8.xlsx
- TableS6.xlsx
- TableS9.xlsx
- TableS10.xlsx
- TableS7.xlsx
- TableS11.xlsx
- TableS12.xlsx
- TableS13.xlsx